

**Decay of a linear pendulum in a collisional gas: Spatially one-dimensional case**Tetsuro Tsuji<sup>1</sup> and Kazuo Aoki<sup>2</sup><sup>1</sup>*Department of Mechanical Science and Bioengineering, Osaka University, Osaka 560-8531, Japan*<sup>2</sup>*Department of Mechanical Engineering and Science and Advanced Research Institute of Fluid Science and Engineering, Kyoto University, Kyoto 615-8540, Japan*

(Received 1 April 2014; published 19 May 2014)

An infinitely wide plate, subject to an external force in its normal direction obeying Hooke's law, is placed in an infinite expanse of a rarefied gas. When the plate is displaced from its equilibrium position and released, it starts in general an oscillatory motion in its normal direction. This is the one-dimensional setting of a linear pendulum considered previously for a collisionless gas and a special Lorentz gas by the present authors [T. Tsuji and K. Aoki, *J. Stat. Phys.* **146**, 620 (2012)]. The motion decays as time proceeds because of the drag force on the plate exerted by the surrounding gas. The long-time behavior of the unsteady motion of the gas caused by the motion of the plate is investigated numerically on the basis of the Bhatnagar-Gross-Krook (BGK) model of the Boltzmann equation with special interest in the rate of the decay of the oscillatory motion of the plate. The result provides numerical evidence that the displacement of the plate decays in proportion to an inverse power of time for large time.

DOI: [10.1103/PhysRevE.89.052129](https://doi.org/10.1103/PhysRevE.89.052129)

PACS number(s): 05.20.Dd, 47.45.Ab, 51.10.+y, 47.11.-j

**I. INTRODUCTION**

We consider a body in an infinite expanse of a gas. The body is subject to an external force obeying Hooke's law (i.e., a restoring force in proportion to the displacement from the equilibrium position) and is movable only along the line parallel to the force. We call this system a *linear pendulum*. If the body is displaced and released with an initial velocity, then it starts an unsteady motion (in general, an oscillation around the equilibrium position), but the motion decays as time proceeds because of the drag force exerted on the body by the surrounding gas. We focus our attention on the rate of the decay of the motion of the body.

If we assume that the drag force is proportional to the speed of the body, the motion of the body decays exponentially in time. However, the drag force is not so simple, and we may expect a different decay rate. This problem has been studied mathematically [1] as well as numerically [2,3] when the surrounding gas is a collisionless gas (a free-molecular gas or the Knudsen gas), i.e., a gas that is so rarefied that collisions between gas molecules can be neglected. These are extensions of the earlier studies of the rate of approach to the final steady motion of the body when it is subject to a constant external force [1,4-7].

The mathematical study in [1] is for the case where the body is a circular disk and the external force, obeying Hooke's law, acts perpendicularly on the disk. The gas molecules are assumed to undergo specular reflection on the disk. Let us denote by  $t_*$  the time variable and by  $X_w(t_*)$  the displacement (with sign) of the disk from the equilibrium position. Then, the external force is expressed as  $-\kappa X_w(t_*)$  with a positive constant  $\kappa$ . Initially, the disk is fixed with displacement  $X_w(0)$ , and the gas is in a uniform equilibrium state at rest. At time  $t_* = 0$ , it is released with an initial velocity (parallel to the external force). Then, the disk starts an unsteady motion, which decays as time proceeds, i.e.,  $X_w(t_*) \rightarrow 0$ . In [1], it is proved that there exist cases where  $X_w(t_*)$  decays monotonically (without oscillation) and that in such cases the decay is slow and algebraic, as described by

$$|X_w(t_*)| \approx C_s / t_*^{d+2}, \quad (1)$$

for sufficiently large  $t_*$ , where  $d$  ( $= 1, 2, 3$ ) is the dimension of the problem and  $C_s$  is a positive constant. Subsequent numerical studies [2,3] confirmed an algebraic decay even in the case with many oscillations. However, since the diffuse-reflection condition, rather than the specular-reflection condition, was assumed in [2,3], the decay rate was different and was proportional to  $1/t_*^{d+1}$ , which is slower than Eq. (1). These algebraically slow decays are attributed to a long-memory effect peculiar to a collisionless gas [1,4]. In such a gas, the molecules that are reflected by the disk at early times may hit the disk again at later times. In contrast to a gas with intermolecular collisions, such molecules transfer information about the disk at an early stage directly to the disk at a later stage and may affect the motion of the disk a long time later. In other words, they give rise to a long-memory effect.

What happens when this long-memory effect is destroyed is exemplified by the special Lorentz gas [3], where a special type of interaction of gas molecules with a background is introduced. It was shown numerically that, in this case, the decay of the motion of the disk is faster than algebraic and more or less exponential in time. This result suggests that a similar fast decay is expected when there are collisions between gas molecules because they also destroy the long-memory effect peculiar to the collisionless gas.

The aim of the present paper is to investigate the same problem, the decay of the linear pendulum, numerically when the gas is collisional. Since this is a moving-boundary problem in which the motion of the disk is coupled with that of the gas, it is very hard to solve the Boltzmann equation with the collision term numerically. Therefore, we simplify our analysis (i) employing the Bhatnagar-Gross-Krook (BGK) model [8,9] instead of the full Boltzmann equation and (ii) restricting ourselves to the spatially one-dimensional case ( $d = 1$ ). In our recent paper [10], we discussed the singularities (discontinuities and weaker singularities) in the solution of the BGK equation produced by a moving boundary and proposed a numerical method capable of describing the propagation of the singularities. We also carried out a preliminary computation of the decay of the linear pendulum in the spatially one-dimensional case. In the present study, which is a continuation

of [10], we adopt two different numerical methods: one is the singularity-capturing method developed in [10] and the other is the semi-Lagrangian method proposed in [11]. We will use the latter method for long-time computation, confirming the accuracy with the former method, which is more accurate but computationally much more expensive.

## II. FORMULATION OF THE PROBLEM

### A. Problem, assumptions, and notations

Let us consider an infinitely wide plate without thickness kept at a uniform and constant temperature  $T_{0*}$  and immersed in an infinite expanse of a rarefied ideal monatomic gas at a uniform equilibrium state at rest with density  $\rho_{0*}$  and temperature  $T_{0*}$ . The plate is subject to an external restoring force obeying Hooke's law in its normal direction (Fig. 1) and is movable in the same direction. Let  $t_*$  be the time variable and  $X_i$  be the Cartesian coordinates in space with the  $X_1$  axis taken perpendicular to the plate, and  $X_1 = 0$  indicates the equilibrium position of the disk. Then, the restoring force  $F_1$  per unit area of the plate is expressed as

$$F_1 = -\mathcal{M}_* \omega_*^2 X_w(t_*), \quad (2)$$

where  $X_w(t_*)$  is the position ( $X_1$  coordinate) of the plate at time  $t_*$ ,  $\mathcal{M}_*$  is the mass density of the plate (the mass of the disk per unit surface), and  $\omega_*$  is the proper frequency of the restoring force.

At time  $t_* = 0$ , the plate is released from a position  $X_1 = X_{w0}$  with an initial velocity  $V_{w0}$  in the  $X_1$  direction. Then, it starts an unsteady motion (in general, an oscillatory motion), but the motion decays as time proceeds because of the drag exerted on the plate by the surrounding gas. We investigate the unsteady motion of the gas as well as that of the plate numerically, with special interest in the long-time behavior and the manner of the decay of the motion of the plate, under the following assumptions:

(i) The behavior of the gas is described by the BGK model of the Boltzmann equation [8,9,12–14].

(ii) The gas molecules undergo diffuse reflection on the plate [12–14]. More specifically, the velocity of the molecules reflected by the plate are distributed according to the (half-range) Maxwellian distribution characterized by the velocity and temperature of the plate and with the density determined in such a way that there is no instantaneous net mass flow across the plate.

(iii) Physical quantities do not depend on  $X_2$  and  $X_3$ .

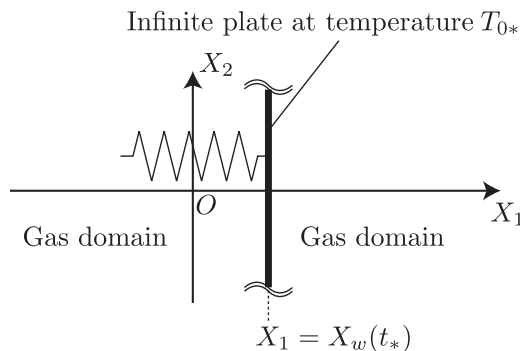


FIG. 1. A plate with a restoring force in a gas.

The present problem is a typical coupling problem of unsteady motion of a rarefied gas and that of a body. Numerical simulation of such types of problem, which may be called coupled moving-boundary problems, are of current interest in rarefied gas dynamics, and different approaches have been attempted (see, e.g., [10,11,15–17]).

Prior to the formulation of the problem, the notations used in the paper are summarized. First, we introduce (and repeat) dimensional variables:  $t_*$  is the time variable,  $X_i$  the Cartesian coordinate system in space (cf. Fig. 1),  $\xi_i$  the molecular velocity,  $X_w$  the position of the plate ( $X_1$  coordinate), and  $V_w$  the velocity of the plate ( $X_1$  direction);  $\rho_*$  is the density of the gas,  $u_{1*}$  the flow velocity of the gas in the  $X_1$  direction (the other two components  $u_{2*}$  and  $u_{3*}$  are assumed to be zero),  $T_*$  the temperature of the gas, and  $f_*$  the velocity distribution function of gas molecules;  $\omega_*$  is the proper frequency contained in the coefficient of Hooke's law,  $\mathcal{M}_*$  the mass of the plate per unit area,  $G_*$  the drag force (in the  $X_1$  direction) acting on the plate per unit area,  $X_{w0}$  the initial position of the plate, and  $V_{w0}$  the initial velocity of the plate.

We choose the reference time  $t_{0*}$  and length  $L_{0*}$  as

$$t_{0*} = 1/\omega_*, \quad L_{0*} = c_{0*}/\omega_*, \quad (3)$$

where  $c_{0*} = \sqrt{2RT_{0*}}$  with  $R$  the gas constant per unit mass ( $R = k_B/m_g$  with the Boltzmann constant  $k_B$  and the mass of a gas molecule  $m_g$ ). Then, we introduce the dimensionless counterparts  $t, x_i, \zeta_i, x_w, v_w, \rho, u_1, T, f, \mathcal{M}, G, x_{w0}$ , and  $v_{w0}$  as follows:

$$\begin{aligned} t &= t_*/t_{0*}, & x_i &= X_i/L_{0*}, & \zeta_i &= \xi_i/c_{0*}, & x_w &= X_w/L_{0*}, \\ v_w &= V_w/c_{0*}, & \rho &= \rho_*/\rho_{0*}, & u_1 &= u_{1*}/c_{0*}, & T &= T_*/T_{0*}, \\ f &= f_*/(\rho_{0*}/c_{0*}^3), & \mathcal{M} &= \mathcal{M}_*/(\rho_{0*}L_{0*}), \\ G &= G_*/(\rho_{0*}c_{0*}^2), & x_{w0} &= X_{w0}/L_{0*}, & v_{w0} &= V_{w0}/c_{0*}. \end{aligned} \quad (4)$$

### B. Basic equations

In the present problem, in which  $u_{2*} = u_{3*} = 0$  and the physical quantities are independent of  $x_2$  and  $x_3$ , we can eliminate the second and third components  $\zeta_2$  and  $\zeta_3$  of the molecular velocity by considering the following marginal velocity distribution functions  $g$  and  $h$  [18]:

$$\begin{aligned} \begin{bmatrix} g(x_1, \zeta_1, t) \\ h(x_1, \zeta_1, t) \end{bmatrix} &= \iint_{-\infty}^{\infty} \begin{bmatrix} 1 \\ \zeta_2^2 + \zeta_3^2 \end{bmatrix} \\ &\times f(x_1, \zeta_1, \zeta_2, \zeta_3, t) d\zeta_2 d\zeta_3. \end{aligned} \quad (5)$$

More specifically, multiplying the original BGK equation and its initial and boundary conditions by 1 and  $\zeta_2^2 + \zeta_3^2$  and integrating the results with respect to  $\zeta_2$  and  $\zeta_3$  from  $-\infty$  to  $\infty$ , we obtain the equations and initial and boundary conditions for  $g$  and  $h$ . That is, the equations are

$$\frac{\partial}{\partial t} \begin{bmatrix} g \\ h \end{bmatrix} + \zeta_1 \frac{\partial}{\partial x_1} \begin{bmatrix} g \\ h \end{bmatrix} = \frac{1}{K} \rho \left( \begin{bmatrix} 1 \\ T \end{bmatrix} M - \begin{bmatrix} g \\ h \end{bmatrix} \right), \quad (6a)$$

$$M = \frac{\rho}{(\pi T)^{1/2}} \exp\left(-\frac{(\zeta_1 - u_1)^2}{T}\right), \quad (6b)$$

$$\begin{bmatrix} \rho \\ \rho u_1 \\ 3\rho T/2 \end{bmatrix} = \int_{-\infty}^{\infty} \begin{bmatrix} g \\ \zeta_1 g \\ (\zeta_1 - u_1)^2 g + h \end{bmatrix} d\zeta_1, \quad (6c)$$

where  $M$  is the one-dimensional local Maxwellian at density  $\rho$ , flow velocity  $u_1$  (in the  $x_1$  direction), and temperature  $T$ ;  $K = (\sqrt{\pi}/2)l_{0*}/L_{0*}$  is a parameter of the order of the Knudsen number  $\text{Kn} = l_{0*}/L_{0*}$ ,  $l_{0*} = (2/\sqrt{\pi})(c_{0*}/A_c\rho_{0*})$  is the mean free path of gas molecules at the equilibrium state at rest at temperature  $T_{0*}$  and density  $\rho_{0*}$ , and  $A_c$  is a positive constant contained in the original BGK model ( $A_c\rho_{0*}$  is the collision frequency of a gas molecule) and is related to the viscosity  $\mu_0$  at temperature  $T_{0*}$  as  $\mu_0 = RT_{0*}/A_c$ . The initial conditions, which correspond to the uniform equilibrium state at rest at temperature  $T_{0*}$  and density  $\rho_{0*}$ , are

$$g(x_1, \zeta_1, 0) = E(\zeta_1), \quad h(x_1, \zeta_1, 0) = E(\zeta_1), \quad (7)$$

where

$$E(\zeta_1) = \pi^{-1/2} \exp(-\zeta_1^2). \quad (8)$$

The boundary conditions on the plate (diffuse reflection) are given by

$$\begin{aligned} g(x_1, \zeta_1, t) &= \sigma_{w\pm}(t)E(\zeta_1 - v_w(t)), \\ h(x_1, \zeta_1, t) &= \sigma_{w\pm}(t)E(\zeta_1 - v_w(t)), \end{aligned} \quad (9)$$

for  $\zeta_1 - v_w(t) \gtrless 0$  at  $x_1 = x_w(t) \pm 0$ ,

where

$$\begin{aligned} \sigma_{w\pm}(t) &= \mp 2\sqrt{\pi} \int_{\zeta_1 - v_w(t) \leq 0} [\zeta_1 - v_w(t)] \\ &\quad \times g(x_w(t) \pm 0, \zeta_1, t) d\zeta_1. \end{aligned} \quad (10)$$

In Eqs. (9) and (10), the upper signs indicate the conditions on the right surface of the plate, and the lower signs those on the left surface (see Fig. 1).

The above initial- and boundary-value problem for the gas should be completed by the equation of motion of the plate and its initial condition, that is,

$$\frac{dx_w}{dt} = v_w(t), \quad \frac{dv_w}{dt} = -x_w(t) - \frac{G}{\mathcal{M}}, \quad (11a)$$

$$x_w(0) = x_{w0}, \quad v_w(0) = v_{w0}. \quad (11b)$$

Here, the dimensionless drag force  $G$  acting on the plate is expressed in terms of the marginal  $g$  as

$$G = G_+ + G_-, \quad (12)$$

$$G_{\pm} = \pm \int_{-\infty}^{\infty} [\zeta_1 - v_w(t)]^2 g(x_w(t) \pm 0, \zeta_1, t) d\zeta_1,$$

where the upper (lower) signs go together.

It should be noted that the problem for the gas, Eqs. (6)–(10), and the problem for the plate, Eqs. (11) and (12), are coupled through the boundary conditions (9) and (10) and the drag (12). We solve these coupled problems numerically by two different methods: One is the method of characteristics proposed in [10] and the other is the semi-Lagrangian method proposed in [11]. As discussed in [10], the oscillating plate continuously produces different types of singularities, such as discontinuities, in the velocity

distribution function in the gas. When the Knudsen number is large, the singularities concentrate in a narrow range of the molecular velocity component  $\zeta_1$  and make the shape of the velocity distribution functions  $g$  and  $h$  very complex. The method of characteristics in [10] is designed in such a way that it can describe the propagation and the localization of the discontinuities and other weaker singularities accurately. In fact, for a collisionless gas, the correct decay rate of the displacement  $x_w(t)$  can be obtained only when such a complex shape is captured correctly [3]. However, since the method is computationally expensive, it is not suitable for obtaining the long-time behavior. The second method, the semi-Lagrangian method, has no such difficulties though it cannot describe the propagation of singularities and the complex shape of the velocity distribution function correctly. As the first step, we confirm the accuracy of the displacement  $x_w(t)$  obtained by the semi-Lagrangian method for a relatively long time interval ( $0 < t \lesssim 10^2$ ) by comparing it with an accurate result based on the method of characteristics. This means that we also confirm that the localization of the singularities and the resulting complex shape of the velocity distribution function do not affect the long-time behavior of  $X_w(t)$ . Then, we only use the semi-Lagrangian method to obtain longer-time behavior (up to  $t \approx 10^4$ ), which is not obtainable by the method of characteristics. This strategy is reasonable because the singularities produced continuously by the oscillating plate decay rather quickly with time for a collisional gas [10], so that they are expected to be harmless for the computation of the very-long-time behavior. Since the method of characteristics is explained in detail in [10], we will omit it in the present paper and focus on the analysis based on the semi-Lagrangian method.

### III. PRELIMINARIES

In this section, we carry out some preliminary transformations of the basic system in order to make them more suitable for the computation using the semi-Lagrangian method.

#### A. Relative coordinate systems

Following Appendix B in [10], we introduce the space coordinate  $\check{x}_1$  relative to  $x_w(t)$ , the molecular velocity  $\check{\zeta}_1$  relative to  $v_w(t)$ , and the new time variable  $\check{t}$ , which is the same as  $t$ , as

$$\check{x}_1 = x_1 - x_w(t), \quad \check{\zeta}_1 = \zeta_1 - v_w(t), \quad \check{t} = t. \quad (13)$$

Then, we define the functions  $\check{\mathcal{F}}$ ,  $\check{\mathcal{H}}$ ,  $\check{\rho}$ ,  $\check{u}_1$ , and  $\check{T}$  for the new variables as follows:

$$\begin{aligned} \check{\mathcal{F}}(\check{x}_1, \check{\zeta}_1, \check{t}) &= \mathcal{F}(\check{x}_1 + x_w(\check{t}), \check{\zeta}_1 + v_w(\check{t}), \check{t}) \\ &\quad - E(\check{\zeta}_1 + v_w(\check{t})) \quad (\mathcal{F} = g, h), \end{aligned} \quad (14a)$$

$$\check{\mathcal{H}}(\check{x}_1, \check{t}) = \mathcal{H}(\check{x}_1 + x_w(\check{t}), \check{t}) \quad (\mathcal{H} = \rho, T),$$

$$\check{u}_1(\check{x}_1, \check{t}) = u_1(\check{x}_1 + x_w(\check{t}), \check{t}) - v_w(\check{t}). \quad (14b)$$

With these new independent and dependent variables, Eqs. (6)–(10) are transformed into the following form: The BGK

equation becomes

$$\left( \frac{\partial}{\partial \check{t}} + \check{\zeta}_1 \frac{\partial}{\partial \check{x}_1} - v_w(\check{t}) \frac{\partial}{\partial \check{\zeta}_1} \right) \begin{bmatrix} \check{g} \\ \check{h} \end{bmatrix} = \frac{1}{K} \begin{bmatrix} Q_g \\ Q_h \end{bmatrix}, \quad (15a)$$

$$\begin{bmatrix} Q_g \\ Q_h \end{bmatrix} = \check{\rho} \left( \begin{bmatrix} 1 \\ \check{T} \end{bmatrix} \check{M} - \begin{bmatrix} 1 \\ 1 \end{bmatrix} E(\check{\zeta}_1 + v_w(\check{t})) - \begin{bmatrix} \check{g} \\ \check{h} \end{bmatrix} \right), \quad (15b)$$

$$\check{M} = \frac{\check{\rho}}{(\pi \check{T})^{1/2}} \exp \left( -\frac{(\check{\zeta}_1 - \check{u}_1)^2}{\check{T}} \right), \quad (15c)$$

$$\begin{bmatrix} \check{\rho} \\ \check{\rho} \check{u}_1 \\ \frac{3}{2} \check{\rho} \check{T} \end{bmatrix} = \begin{bmatrix} 1 \\ -v_w(\check{t}) \\ \frac{3}{2} + v_w^2(\check{t}) - \check{\rho} \check{u}_1^2 \end{bmatrix} + \int_{-\infty}^{\infty} \begin{bmatrix} \check{g} \\ \check{\zeta}_1 \check{g} \\ \check{\zeta}_1^2 \check{g} + \check{h} \end{bmatrix} d\check{\zeta}_1, \quad (15d)$$

the initial condition is

$$\check{g}(\check{x}_1, \check{\zeta}_1, 0) = 0, \quad \check{h}(\check{x}_1, \check{\zeta}_1, 0) = 0, \quad (16)$$

and the boundary condition is

$$\begin{bmatrix} \check{g} \\ \check{h} \end{bmatrix}(\check{x}_1, \check{\zeta}_1, \check{t}) = [\check{\sigma}_{w\pm}(\check{t}) E(\check{\zeta}_1) - E(\check{\zeta}_1 + v_w(\check{t}))] \begin{bmatrix} 1 \\ 1 \end{bmatrix},$$

for  $\check{\zeta}_1 \geq 0$  at  $\check{x}_1 = \pm 0$ , (17a)

$$\check{\sigma}_{w\pm}(\check{t}) = \check{\sigma}_{\text{eq}\pm}(v_w(\check{t})) \mp 2\sqrt{\pi} \int_{\check{\zeta}_1 \leq 0} \check{\zeta}_1 \check{g}(\pm 0, \check{\zeta}_1, \check{t}) d\check{\zeta}_1, \quad (17b)$$

$$\check{\sigma}_{\text{eq}\pm}(x) = e^{-x^2} \pm x \sqrt{\pi} \operatorname{erfc}(\mp x). \quad (17c)$$

The drag force (12) is transformed to

$$G(\check{t}) = \int_{-\infty}^{\infty} \check{\zeta}_1^2 \check{g}(+0, \check{\zeta}_1, \check{t}) d\check{\zeta}_1 - \int_{-\infty}^{\infty} \check{\zeta}_1^2 \check{g}(-0, \check{\zeta}_1, \check{t}) d\check{\zeta}_1. \quad (18)$$

The initial- and boundary-value problem, Eqs. (15)–(18) together with Eq. (11), is that for the plate at rest, and the effect of its unsteady motion appears as an external force acting on the gas molecules, i.e., the third term on the left-hand side of Eq. (15a). In the long-time limit  $\check{t} \rightarrow \infty$ , each physical quantity approaches its equilibrium value, e.g.,  $\lim_{\check{t} \rightarrow \infty} x_w(\check{t}) = 0$ ,  $\lim_{\check{t} \rightarrow \infty} v_w(\check{t}) = 0$ , and  $\lim_{\check{t} \rightarrow \infty} g(\check{x}_1, \check{\zeta}_1, \check{t}) = E(\check{\zeta}_1 + v_w(\check{t})) = E(\check{\zeta}_1)$ . Therefore, handling the deviations  $\check{g}$  and  $\check{h}$  from the equilibrium has more advantage for accurate computation for large  $t$ .

### B. Integration along characteristics

Now we integrate Eq. (15) along its characteristics from  $\check{t}_0$  to  $\check{t}$  ( $> \check{t}_0$ ) to obtain the following form (cf. Fig. 2):

$$\begin{aligned} & \begin{bmatrix} \check{g} \\ \check{h} \end{bmatrix}(\check{x}_1, \check{\zeta}_1, \check{t}) \\ &= \begin{bmatrix} \check{g} \\ \check{h} \end{bmatrix}(W(\check{t}_0; \check{x}_1, \check{\zeta}_1, \check{t}), Z(\check{t}_0; \check{x}_1, \check{\zeta}_1, \check{t}), \check{t}_0) \\ &+ \frac{1}{K} \int_{\check{t}_0}^{\check{t}} \begin{bmatrix} Q_g \\ Q_h \end{bmatrix}(W(s; \check{x}_1, \check{\zeta}_1, \check{t}), Z(s; \check{x}_1, \check{\zeta}_1, \check{t}), s) ds, \end{aligned} \quad (19a)$$

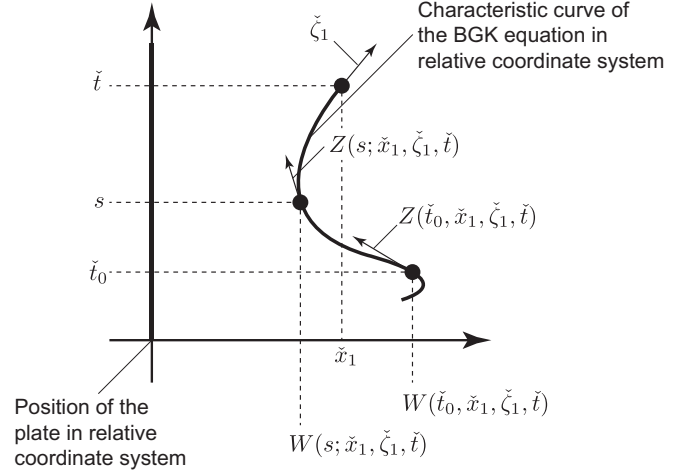


FIG. 2. Schematic figure for integration along characteristics in the  $\check{x}_1\check{t}$  plane. For a given set of  $(\check{x}_1, \check{\zeta}_1, \check{t})$ , Eq. (19b) describes the trajectory of a molecule in the  $\check{x}_1\check{t}$  plane with  $s$  as a parameter. The slope of the arrow in the figure corresponds to the molecular velocity at the origin of the arrow.

$$W(s; \check{x}_1, \check{\zeta}_1, \check{t}) = \check{x}_1 - [\check{\zeta}_1 + v_w(\check{t})](\check{t} - s) + x_w(\check{t}) - x_w(s), \quad (19b)$$

$$Z(s; \check{x}_1, \check{\zeta}_1, \check{t}) = \check{\zeta}_1 + v_w(\check{t}) - v_w(s). \quad (19c)$$

Concerning Eq. (19a), if we integrate, respectively, (the upper line), (the upper line)  $\times \check{\zeta}_1$ , and (the upper line)  $\times \check{\zeta}_1^2 +$  (the lower line) and note that there is no contribution from  $Q_g$  and  $Q_h$ , then we obtain the conservation laws in the form corresponding to Eq. (19a). That is,

$$M_0 = \int_{-\infty}^{\infty} \check{g}(W(\check{t}_0; \check{x}_1, \check{\zeta}_1, \check{t}), Z(\check{t}_0; \check{x}_1, \check{\zeta}_1, \check{t}), \check{t}_0) d\check{\zeta}_1, \quad (20a)$$

$$M_1 = \int_{-\infty}^{\infty} \check{\zeta}_1 \check{g}(W(\check{t}_0; \check{x}_1, \check{\zeta}_1, \check{t}), Z(\check{t}_0; \check{x}_1, \check{\zeta}_1, \check{t}), \check{t}_0) d\check{\zeta}_1, \quad (20b)$$

$$M_2 = \int_{-\infty}^{\infty} \check{\zeta}_1^2 \check{g}(W(\check{t}_0; \check{x}_1, \check{\zeta}_1, \check{t}), Z(\check{t}_0; \check{x}_1, \check{\zeta}_1, \check{t}), \check{t}_0) d\check{\zeta}_1 + \int_{-\infty}^{\infty} \check{h}(W(\check{t}_0; \check{x}_1, \check{\zeta}_1, \check{t}), Z(\check{t}_0; \check{x}_1, \check{\zeta}_1, \check{t}), \check{t}_0) d\check{\zeta}_1, \quad (20c)$$

where we have put

$$\begin{aligned} M_0 &= \check{\rho} - 1, \quad M_1 = \check{\rho} \check{u}_1 + v_w(\check{t}), \\ M_2 &= \frac{3}{2} \check{\rho} \check{T} - \left( \frac{3}{2} + v_w^2(\check{t}) - \check{\rho} \check{u}_1^2 \right). \end{aligned} \quad (21)$$

The conservation laws of this form are useful for the numerical computation of the collision term [the terms containing  $Q_g$  and  $Q_h$  on the right-hand side of Eq. (19a); see the last paragraph of procedure (C) in the Appendix, subsection 3].

We solve the initial- and boundary-value problem, Eqs. (15)–(18) with Eq. (11), numerically by the semi-Lagrangian method using the form (19) rather than Eq. (15). Since the detailed description of the numerical method is

tedious, we put its outline in the Appendix and move on to the results of computation.

#### IV. RESULTS OF NUMERICAL ANALYSIS

In this section, the numerical results obtained by the two methods are presented. The results are shown in the original coordinate system  $(x_1, \zeta_1, t)$  rather than the relative coordinate system  $(\check{x}_1, \check{\zeta}_1, \check{t})$  [see Eqs. (13) and (14)]. First, the method of characteristics [10] is used to investigate the singularities produced by the moving plate, which are inherent to moving-boundary problems (Sec. IV A). Then, we compare the results by the two methods (Sec. IV B) for relatively large times  $t > 10^2$  to confirm the accuracy of the semi-Lagrangian method. Finally, the semi-Lagrangian method is used to investigate the very-long-time behavior (up to  $t = 10^4$ ) of the displacement  $|x_w(t)|$  of the plate (Sec. IV C).

Here we note that the parameters characterizing the present problem are the dimensionless initial displacement  $x_{w0}$  and velocity  $v_{w0}$  of the plate, the dimensionless density  $\mathcal{M}$  of the plate, and the effective Knudsen number  $K$ . In the present paper, we only consider the case where the initial velocity of the plate is zero ( $v_{w0} = 0$ ).

##### A. Velocity distribution function

In our previous paper [10], we considered two problems: One is the present problem where the oscillation of the plate decays (Problem II there), and the other is the problem where the plate undergoes a forced (not decaying) oscillation (Problem I there). The latter is the problem of nonlinear acoustic wave propagation in a half space (see also [19]). For this problem, we explained the mechanism of the production of the singularities in the solution by the oscillating plate and

their localization. We also demonstrated the resulting complex shape of the velocity distribution function. Therefore, we avoid repeating similar behavior for the decaying oscillation in the present problem, showing only a few examples.

In Fig. 3, we show the marginal velocity distribution function  $g(x_1, \zeta_1, t)$  on the right side of the plate  $[x_1 = x_w(t) + 0]$  as a function of  $\zeta_1$  at  $t = 10$  [Figs. 3(a)–3(d)] and  $t = 20$  [Figs. 3(e)–3(h)] for  $x_{w0} = 0.1$ ,  $v_{w0} = 0$ ,  $\mathcal{M} = 2$ , and  $K = 10$  and 1. The solid line indicates the result for  $K = 10$  and the bold dashed line that for  $K = 1$ ; thin vertical dashed line represents discontinuities. Panels (b), (c), and (d) are the closeups of panels (a), (b), and (c) around  $\zeta_1 = 0$ , respectively, and panels (f), (g), and (h) are the closeups of panels (e), (f), and (g), respectively.

According to [10], the velocity distribution function in the gas (including that on the plate) in the problems where the plate is oscillating in its normal direction has the following properties:

**P1** The velocity distribution function may have several discontinuities (and also the discontinuities of its derivative with respect to  $\zeta_1$ ) depending on the time and position under consideration and on the trajectory of the plate.

**P2** These discontinuities accumulate around  $\zeta_1 = 0$  as time goes on (localization).

**P3** The derivative of the velocity distribution function with respect to  $\zeta_1$  may become large (i.e.,  $|\partial g / \partial \zeta_1| \gg 1$ ) at the discontinuities.

**P4** The discontinuity decays as time goes on in such a manner that

$$\text{Magnitude of discontinuity} \lesssim C \exp(-\rho_{\min} t / K), \quad (22)$$

where  $C$  is a positive constant, and  $\rho_{\min}$  is the minimum of  $\rho$  along the molecular trajectory.

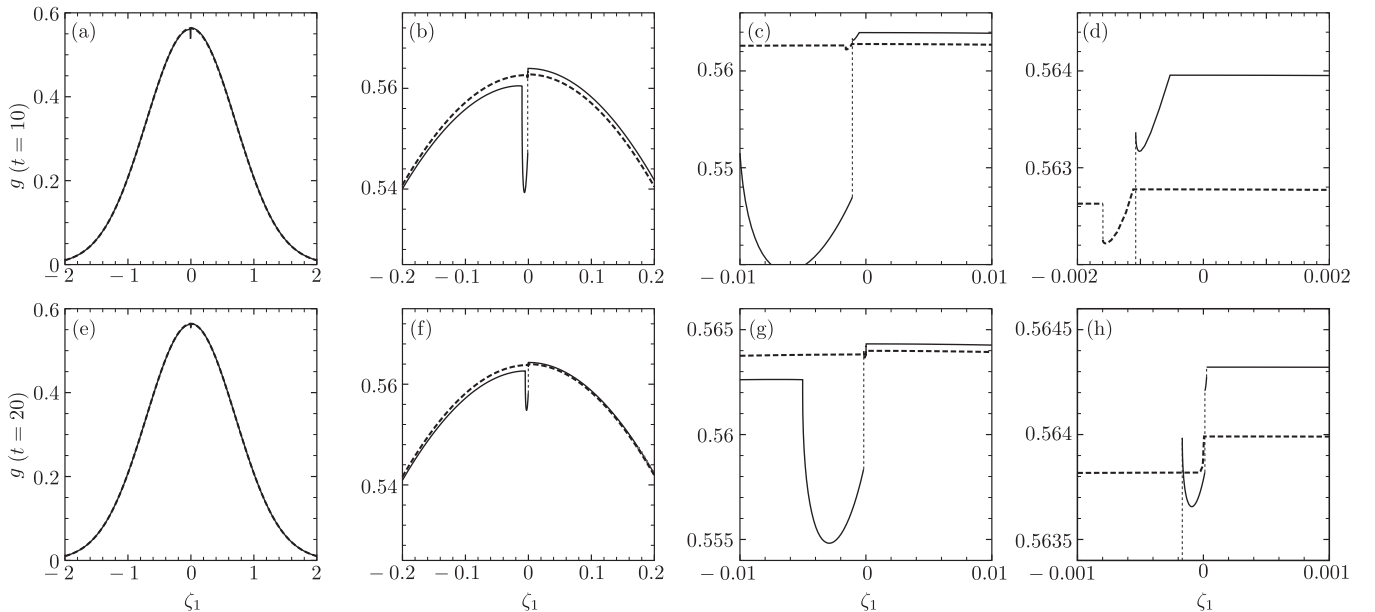


FIG. 3. Snapshot of the velocity distribution function  $g(x_1, \zeta_1, t)$  versus  $\zeta_1$  on the right side of the plate  $[x_1 = x_w(t) + 0]$  for  $x_{w0} = 0.1$ ,  $v_{w0} = 0$ ,  $\mathcal{M} = 2$ , and  $K = 10$  and 1. The solid line indicates the result for  $K = 10$  and the bold dashed line that for  $K = 1$ ; the thin vertical dashed line represents discontinuities. Panels (a)–(d) are at  $t = 10$ , and panels (e)–(h) at  $t = 20$ . Panels (b), (c), and (d) are the closeups of panels (a), (b), and (c) around  $\zeta_1 = 0$ , respectively, and panels (f), (g), and (h) are the closeups of panels (e), (f), and (g), respectively.

As one can see from Figs. 3(b)–3(d) and 3(f)–3(h), the velocity distribution function for  $K = 10$  is discontinuous. In particular, Fig. 3(h) shows that there are some discontinuities (property **P1**) at two different molecular velocities near  $\zeta_1 = 0$  (property **P2**). The gradient  $|\partial g / \partial \zeta_1|$  is steep at some points for  $K = 10$ , e.g.,  $\zeta_1 \approx -0.001$  in panel (d),  $\zeta_1 \approx -0.005$  in panel (g), and  $\zeta_1 \approx -0.00016$  in panel (h) (property **P3**). These steep gradients actually diverge when  $K \rightarrow \infty$  (weak singularities; see [10]). In contrast, for an intermediate Knudsen number,  $K = 1$ , we hardly see the discontinuities because more frequent collisions between gas molecules tend to attenuate the discontinuities (property **P4**). The decay of the discontinuities with time (property **P4**) can be seen by comparing panels (b) ( $t = 10$ ) and (f) ( $t = 20$ ). Even for  $K = 1$ , we still observe a steep gradient in Fig. 3(h) though the variation in  $g$  across this steep gradient is quite small (it is about  $2 \times 10^{-4}$ ).

### B. Comparison between the two methods

In [10], in addition to the accurate method of characteristics, we also tried a finite-difference method with the essentially nonoscillatory (ENO) scheme. For the problem of a forced oscillation (Problem I in [10]), we demonstrated that the latter method was not able to capture the complex shape of the velocity distribution function for large and intermediate Knudsen numbers. Nevertheless, concerning macroscopic quantities, it could give surprisingly good results even for large Knudsen numbers. Therefore, we also applied this method to the present problem of decaying oscillation in [10] and found that it was not able to reproduce the algebraic decay rate  $x_w(t) \approx \text{const} \times t^{-2}$  [see the paragraph containing Eq. (1)] for a collisionless gas ( $\text{Kn} = \infty$ ). However, for a collisional gas with finite  $\text{Kn}$ , it could give good results for the time evolution of the displacement  $x_w(t)$ .

These facts gave us hope to tackle the problem of finding the decay rate of the plate using, in place of the computationally expensive method of characteristics, a convenient method that cannot describe the singularities in the velocity distribution function accurately but is expected to give good results for macroscopic quantities and time evolution of the displacement  $x_w(t)$ . We have chosen the semi-Lagrangian method for this purpose. This method has several advantages compared with the finite-difference method with the ENO scheme attempted in [10]. For instance, since the ENO scheme is basically an explicit method, we have severe restrictions on the grid size and time step. In contrast, the semi-Lagrangian method is much more tolerant, so that we can use very fine grids near the plate and coarse grids in the far field and very small time steps at the initial stages and larger time steps at later times. Thus, we can carry out an accurate long-time computation.

As one can see from Fig. 3, the magnitude of discontinuities decreases for larger  $t$  or for smaller  $K$  (property **P4**). Therefore, we expect that the macroscopic quantities, such as the drag  $G$ , may not suffer from the complex shape of the velocity distribution function with discontinuities for larger  $t$  or for smaller  $K$ . This also supports the use of the semi-Lagrangian method for the long-time computation to find out the decay rate of the displacement  $x_w(t)$ .

In this subsection, we validate the semi-Lagrangian method by the comparison of the results based on it with those obtained

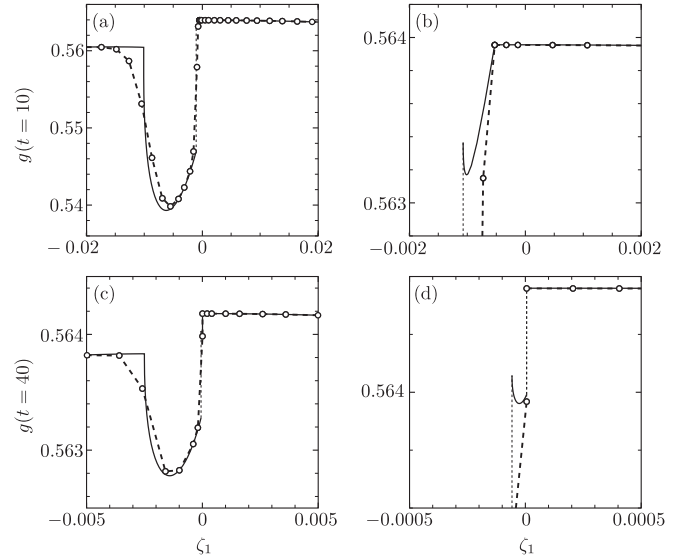


FIG. 4. Comparison between the results by the method of characteristics and those by the semi-Lagrangian method: Snapshot of the velocity distribution function  $g(x_1, \zeta_1, t)$  versus  $\zeta_1$  near  $\zeta_1 = 0$  on the right side of the plate [ $x_1 = x_w(t) + 0$ ] for  $x_{w0} = 0.1$ ,  $v_{w0} = 0$ ,  $\mathcal{M} = 2$ , and  $K = 10$ . Panels (a) and (b) are at  $t = 10$ , and panels (c) and (d) at  $t = 40$ . Panels (b) and (d) are the closeups of panels (a) and (c) around  $\zeta_1 = 0$ , respectively. The bold solid line indicates the results based on the method of characteristics and the small circles with the bold dashed line those based on the semi-Lagrangian method; the thin vertical dashed line represents discontinuities.

by the method of characteristics, which is summarized in Figs. 4–6 and Table I. Figure 4 shows the comparison for the snapshots of the velocity distribution function  $g(x_1, \zeta_1, t)$  versus  $\zeta_1$  near  $\zeta_1 = 0$  on the right side of the plate [ $x_1 = x_w(t) + 0$ ] for  $x_{w0} = 0.1$ ,  $v_{w0} = 0$ ,  $\mathcal{M} = 2$ , and  $K = 10$ . Panels (a) and (b) are at  $t = 10$ , and panels (c) and (d) at  $t = 40$ . Panels (b) and (d) are the closeups of panels (a) and (c) around  $\zeta_1 = 0$ , respectively. The bold solid line indicates the results based on the method of characteristics and the small circles connected by the bold dashed straight line those based on the semi-Lagrangian method. Obviously, the semi-Lagrangian method cannot describe the steep change occurring near  $\zeta_1 = 0$ . However, the discrepancy takes place only in the narrow range of  $\zeta_1$ , so that we can expect that this discrepancy does not show up in the macroscopic quantities (note that this discrepancy affects the results qualitatively in the case of a collisionless gas [10]).

Figure 5 shows the comparison for the profiles (with respect to the original space coordinate  $x_1$ ) of the macroscopic quantities  $\rho$ ,  $u_1$ , and  $T$  at different times for  $x_{w0} = 0.1$ ,  $v_{w0} = 0$ ,  $\mathcal{M} = 2$ , and  $K = 1$ . Panels (a) and (d) are for  $\rho - 1$ , panels (b) and (e) are for  $u_1$ , and panels (c) and (f) are for  $T - 1$ . Panels (a)–(c) show the results at  $t = 5, 10, 15$ , and panels (d)–(f) those at  $t = 25, 50, 100$ . In the figure, the bold dashed line indicates the results based on the method of characteristics and the solid line those based on the semi-Lagrangian method. The two results agree very well at each time  $t$ . This supports our expectation mentioned at the end of the preceding paragraph.

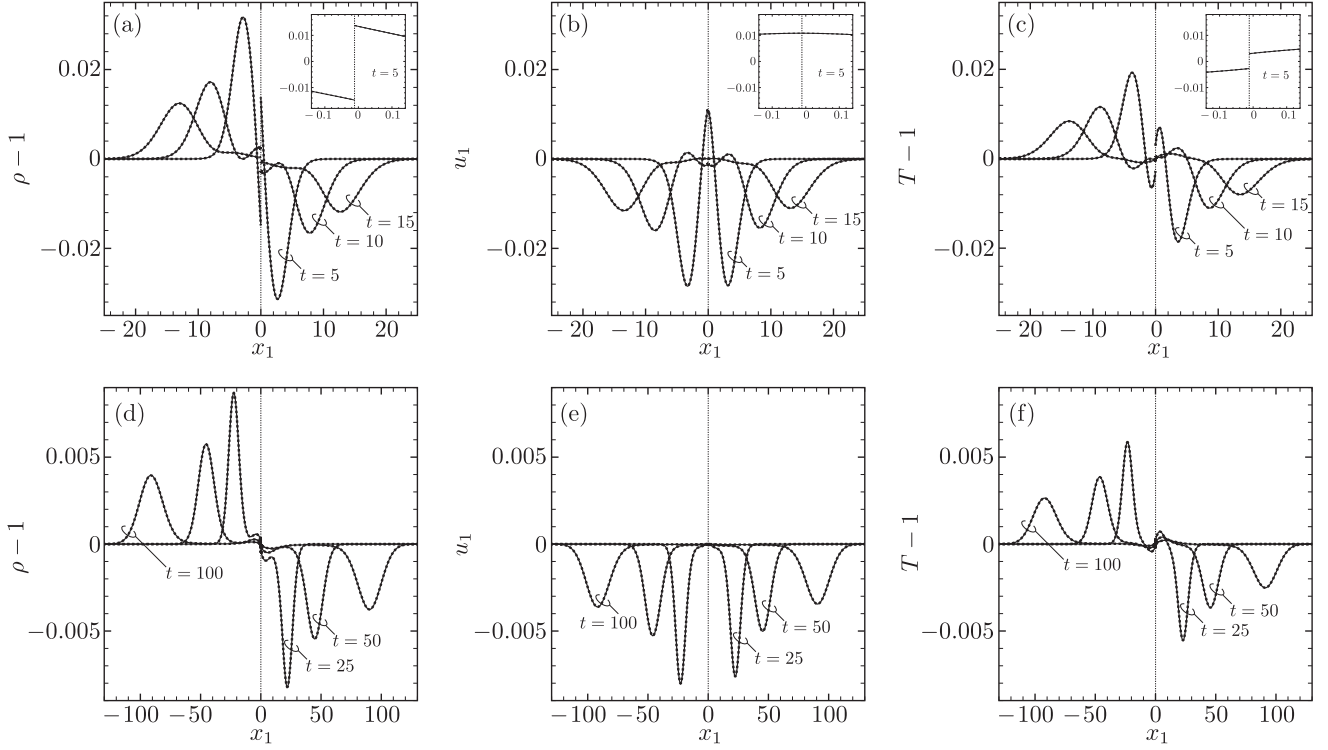


FIG. 5. Comparison between the results by the method of characteristics and those by the semi-Lagrangian method: profiles of the macroscopic quantities at different times for  $x_{w0} = 0.1$ ,  $v_{w0} = 0$ ,  $\mathcal{M} = 2$ , and  $\mathbf{K} = 1$ . (a) and (d)  $\rho - 1$ , (b) and (e)  $u_1$ , (c) and (f)  $T - 1$ . Panels (a)–(c) show the results at  $t = 5, 10, 15$ , and panels (d)–(f) those at  $t = 25, 50, 100$ . The bold dashed line indicates the results based on the method of characteristics, and the solid line those based on the semi-Lagrangian method; the thin vertical dashed line indicates the position of the plate. In panels (a)–(c), the closeups around  $x_1 = 0$  are also shown.

Figure 6 shows the comparison of the time evolution of the amplitude  $|x_w(t)|$  and the speed  $|v_w(t)|$  of the plate for the following four cases:

- case 1:  $x_{w0} = 0.1$ ,  $v_{w0} = 0$ ,  $\mathcal{M} = 2$ , and  $\mathbf{K} = 1$ ,
  - case 2:  $x_{w0} = 0.01$ ,  $v_{w0} = 0$ ,  $\mathcal{M} = 2$ , and  $\mathbf{K} = 1$ ,
  - case 3:  $x_{w0} = 0.1$ ,  $v_{w0} = 0$ ,  $\mathcal{M} = 2$ , and  $\mathbf{K} = 10$ ,
  - case 4:  $x_{w0} = 0.01$ ,  $v_{w0} = 0$ ,  $\mathcal{M} = 2$ , and  $\mathbf{K} = 10$ .
- (23)

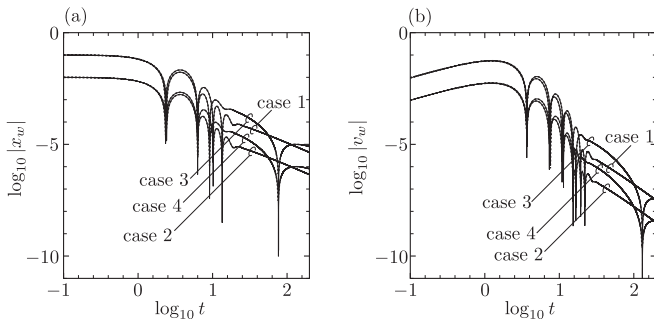


FIG. 6. Comparison between the results by the method of characteristics and those by the semi-Lagrangian method: Time evolution of the amplitude  $|x_w(t)|$  and the speed  $|v_w(t)|$  of the plate for cases 1–4 [cf. Eq. (23)]. (a)  $|x_w(t)|$ , (b)  $|v_w(t)|$ .  $\log_{10}|x_w(t)|$  and  $\log_{10}|v_w(t)|$  are plotted versus  $\log_{10}t$ . Here, the bold dashed line indicates the result by the method of characteristics and the solid line that by the semi-Lagrangian method.

In the figure,  $\log_{10}|x_w(t)|$  and  $\log_{10}|v_w(t)|$  are plotted versus  $\log_{10}t$ ; the bold dashed line indicates the result by the method of characteristics and the solid line that by the semi-Lagrangian method. The two lines agree very well.

Let us denote by  $x_w^{(s)}$  the displacement  $x_w(t)$  obtained by the semi-Lagrangian method and by  $x_w^{(c)}$  that by the method of characteristics, and let us define the relative difference between two methods as

$$E_{\text{dif}} = \left| \frac{\log_{10}|x_w^{(s)}| - \log_{10}|x_w^{(c)}|}{\log_{10}|x_w^{(s)}|} \right|. \quad (24)$$

In Table I, we show  $E_{\text{dif}}$  at five different  $t$  for cases 1–4 of Eq. (23).

TABLE I. Relative difference  $E_{\text{dif}}(t)$  between  $|x_w|$  obtained by two methods.

		$E_{\text{dif}}(t)$			
$t$	$\log_{10}t$	case 1	case 2	case 3	case 4
1	0	2.03(−5) <sup>a</sup>	1.13(−5)	1.15(−5)	6.22(−6)
5	0.698	6.13(−5)	4.29(−5)	1.41(−5)	8.49(−6)
10	1	6.11(−4)	5.03(−4)	1.37(−4)	8.93(−5)
50	1.698	1.67(−4)	1.28(−4)	1.54(−3)	1.30(−3)
100	2	7.29(−5)	4.33(−5)	2.37(−4)	1.74(−4)

<sup>a</sup>Read as  $2.03 \times 10^{-5}$ .

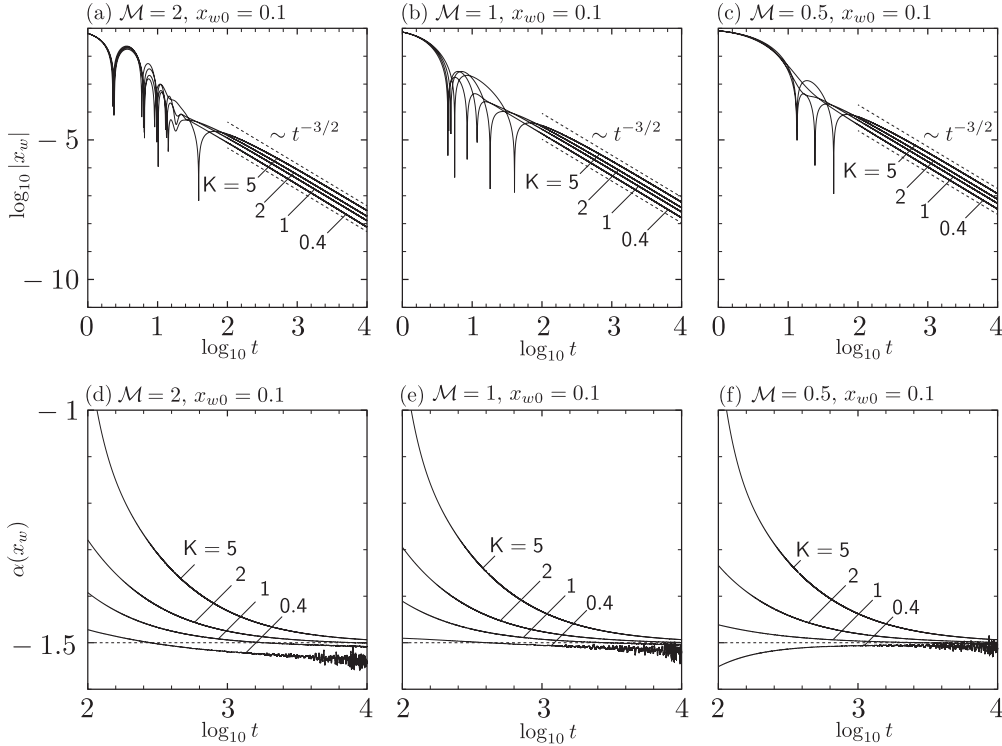


FIG. 7.  $\log_{10}|x_w|$  versus  $\log_{10}t$  for long times at several  $K$  for  $x_{w0} = 0.1$ ,  $v_{w0} = 0$ . (a)  $\mathcal{M} = 2$ , (b)  $\mathcal{M} = 1$ , (c)  $\mathcal{M} = 0.5$ . Panels (d), (e), and (f) show, respectively, the gradient of the curves in panels (a), (b), and (c) [cf. Eq. (25)].

From the observations given above, we may conclude that the semi-Lagrangian method is reliable for the long-time computation to find the decay rate of  $|x_w(t)|$ . This also confirms the following important fact. As pointed out in [3,10], in the case of a collisionless gas, the complex shape of the velocity distribution function caused by the localized discontinuities, which arises in a very small range of the molecular velocity  $\zeta_1$  that shrinks as time proceeds, has a crucial effect on the decay rate of the amplitude  $|x_w(t)|$  as  $t \rightarrow \infty$ . In fact, the finite-difference method that was not able to describe the complex shape failed to give the correct decay rate  $|x_w(t)| \approx \text{const} \times t^{-2}$  [10]. In contrast, in the case of a collisional gas, the localized discontinuities do not affect the decay rate of  $|x_w(t)|$  even when the Knudsen number is relatively high (e.g.,  $K = 10$ ).

### C. Long-time behavior and decay rate of amplitude

Finally, in this subsection, we discuss the long-time behavior of the displacement  $x_w(t)$  of the plate and its decay rate. The results that will be presented here are all obtained by the semi-Lagrangian method. Let us denote by  $\alpha(x_w)$  the gradient of  $\log_{10}|x_w(t)|$  with respect to  $\log_{10}t$ , i.e.,

$$\alpha(x_w) = \frac{d \log_{10}|x_w|}{d \log_{10}t}, \quad (25)$$

which corresponds to an exponent of  $|x_w|$ , namely, if  $|x_w| \propto t^{-n}$ , then we have  $\alpha(x_w) = -n$ . Figures 7(a), 7(b), and 7(c) show  $\log_{10}|x_w|$  versus  $\log_{10}t$  for long times at several  $K$  for  $x_{w0} = 0.1$ ,  $v_{w0} = 0$  and for  $\mathcal{M} = 2$  (a), 1 (b), and 0.5 (c). Figures 7(d), 7(e), and 7(f) demonstrate the time evolution of the gradients of the curves, i.e.,  $\alpha(x_w)$  versus  $\log_{10}t$ , in

Figs. 7(a), 7(b), and 7(c), respectively. Figures 8(a), 8(b), and 8(c) show  $\log_{10}|x_w|$  versus  $\log_{10}t$  at several  $K$  for  $\mathcal{M} = 1$ ,  $v_{w0} = 0$  and for  $x_{w0} = 0.2$  (a), 0.01 (b), and 0.001 (c). Figures 8(d), 8(e), and 8(f) demonstrate  $\alpha(x_w)$  versus  $\log_{10}t$  for the curves in Figs. 8(a), 8(b), and 7(c), respectively. The values of  $\alpha(x_w)$  at  $\log_{10}t = 4$  ( $t = 10^4$ ) in the cases presented in Figs. 7(d)–7(f) and Figs. 8(d)–8(f) are shown in Tables II and III, respectively.

It is seen from Figs. 7 and 8 that for all the cases except  $K = 0.4$ ,  $\alpha(x_w)$  tends, on the whole, to approach  $-3/2$ . This means that the amplitude  $|x_w|$  is likely to decrease in proportion to an inverse power of time as

$$|x_w| \approx Ct^{-3/2} \quad \text{for } t \gg 1, \quad (26)$$

where  $C$  is a positive constant. On the other hand, for  $K = 0.4$ , the curves of  $\alpha(x_w)$  exhibit fluctuations for  $\log_{10}t \gtrsim 3.2$ . In addition, these curves, except in Fig. 7(f), cross the line of  $-3/2$  from above and stay below the line (overshoot) (in this context, we consider the curves averaged out over the fluctuations when

TABLE II. Values of  $\alpha(x_w)$  at  $\log_{10}t = 4$  ( $t = 10^4$ ) for the cases presented in Fig. 7 ( $x_{w0} = 0.1$  and  $v_{w0} = 0$ ).

K	$-\alpha(x_w)$		
	$\mathcal{M} = 2$	$\mathcal{M} = 1$	$\mathcal{M} = 0.5$
5	1.493	1.493	1.493
2	1.500	1.499	1.499
1	1.509	1.506	1.504
0.4	1.541	1.521	1.513

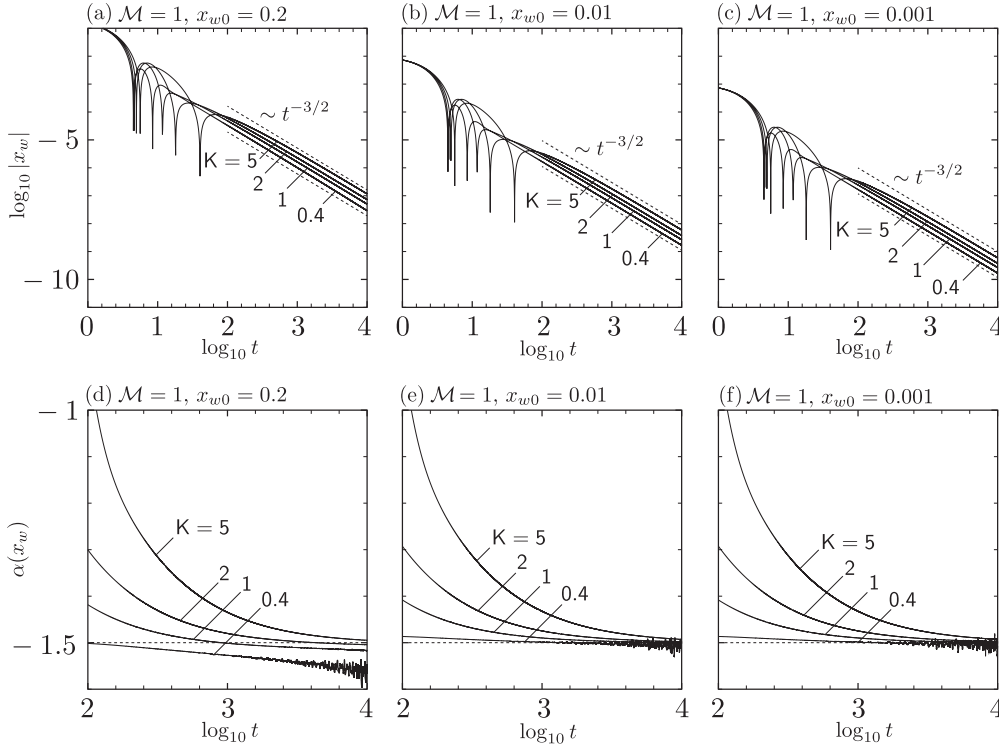


FIG. 8.  $\log_{10}|x_w|$  versus  $\log_{10}t$  for long times at several  $K$  for  $\mathcal{M} = 1$ ,  $v_{w0} = 0$ . (a)  $x_{w0} = 0.2$ , (b)  $x_{w0} = 0.01$ , and (c)  $x_{w0} = 0.001$ . Panels (d), (e), and (f) show, respectively, the gradient of the curves in panels (a), (b), and (c) [cf. Eq. (25)].

they fluctuate). In the present computation up to  $\log_{10}t = 4$ , it is not clear whether or not the curves that have crossed the line of  $-3/2$  from above approach the line from below. If we give a closer look at Figs. 7(d)–7(f) and 8(d) and refer to Tables II and III, we notice that some curves for  $K = 1$  and 2 also show slight overshoot. The overshoot tends to disappear for larger  $K$ , smaller  $\mathcal{M}$ , or smaller  $x_{w0}$ . The fluctuations of the curves for  $K = 0.4$  at large times ( $\log_{10}t \gtrsim 3.2$ ) may be attributed to numerical inaccuracy caused by the fact that  $|x_w(t)|$  becomes very small when  $\log_{10}t$  approaches 4. We have also checked that, with coarser grid systems, the approach of  $\alpha(x_w)$  to  $-3/2$  for larger  $K$  becomes worse and less clear. We must say that the values of  $\mathcal{M}$  chosen in Figs. 7 and 8 are slightly unrealistic, since the area density of the plate is more or less the same as the density of the gas. This is because realistic large values of  $\mathcal{M}$  lead to many oscillations before the manner of decay can be seen, so that an extremely long time computation, which is practically impossible, is required to find the correct decay rate. However, at least for the values of  $\mathcal{M}$  used in Figs. 7

and 8 and for intermediate and large values of  $K$ , we were able to provide numerical evidence supporting Eq. (26).

The manner of the decay given by Eq. (26) for a collisional gas is different either from that for a collisionless gas ( $|x_w(t)| \approx \text{const} \times t^{-2}$ ) [3] or from the almost exponential decay for a special Lorentz gas [3]. Since the collisions between gas molecules destroy the long-tail memory peculiar to a collisionless gas in a way similar to the case of the special Lorentz gas, which was indeed a toy model of the collisional gas, we expected a faster decay in the case of a collisional gas. On the contrary, the obtained decay rate (26) is even slower than that for a collisionless gas.

## V. CONCLUDING REMARKS

In the present study, we considered the one-dimensional case of the linear pendulum in a rarefied collisional gas, that is, unsteady motion of an infinitely wide plate in an infinite expanse of a rarefied gas under the action of an external force in the direction normal to the plate obeying Hooke's law. On the basis of the BGK model of the Boltzmann equation, we have investigated the long-time behavior of the motion of the gas as well as that of the plate numerically with special interest in the manner of decay of the motion of the plate caused by the drag force exerted on it by the surrounding gas.

As discussed in detail in [10], the oscillatory motion of the plate produces discontinuities and other weaker singularities in the velocity distribution function, which are localized as time proceeds and make the shape of the velocity distribution function complex. In the same paper, we developed a numerical method (method of characteristics) that is able to describe the

TABLE III. Values of  $\alpha(x_w)$  at  $\log_{10}t = 4$  ( $t = 10^4$ ) for the cases presented in Fig. 8 ( $\mathcal{M} = 1$  and  $v_{w0} = 0$ ).

K	$-\alpha(x_w)$		
	$x_{w0} = 0.2$	$x_{w0} = 0.01$	$x_{w0} = 0.001$
5	1.494	1.492	1.492
2	1.504	1.497	1.498
1	1.518	1.501	1.500
0.4	1.567	1.497	1.507

complex shape as well as the propagation of singularities. In the present paper, we first demonstrated the complex shape of the velocity distribution function on the plate with decaying oscillation using the method of characteristics (Sec. IV A). The method is accurate, but it is computationally expensive and is not suitable for long-time computation that is required to see the decay rate. For this purpose, we adopt the semi-Lagrangian method proposed in [11]. The method cannot describe the velocity distribution function of complex shape precisely but was hoped to give the correct long-time behavior of the motion of the plate. In fact, we have confirmed its accuracy by comparing its result with the result obtained by the method of characteristics for relatively long time (Sec. IV B). Finally, we carried out computation using the semi-Lagrangian method for a very long time interval, up to  $t = 10^4$  (Sec. IV C). As the result, we obtain numerical evidence showing the decay of the displacement as given by Eq. (26). This decay rate is much slower than the case of a special Lorentz gas that is a toy model for a collisional gas and even slower than the slow decay in the case of a collisionless gas [10].

It should be mentioned that a three-dimensional linear pendulum with a sphere as the body subject to an external restoring force placed in a Stokes fluid was investigated analytically in [20]. In this case, it was proved that the displacement of the sphere  $x_w$  decays as  $|x_w| \approx \text{const} \times t^{-3/2}$  as  $t \rightarrow \infty$ . Therefore, the study of the present problem in the fluid-dynamic limit, perhaps using the Navier-Stokes equations for a compressible fluid, would be an interesting problem.

Finally, we should mention that the present problem has some relevance to the piston problem, a fundamental problem in statistical physics (see e.g., [21–23] and the references therein). In [21–23], a movable piston placed in a gas occupying a finite domain is considered, and unsteady motion of the piston caused by the difference in the initial state of the gas in both sides of the piston is investigated. In contrast, in the present problem, the plate is placed in an infinite expanse of a gas in an equilibrium state at rest, and its unsteady motion is caused by the initial displacement and the restoring force acting on the plate.

## ACKNOWLEDGMENTS

T.T. wishes to thank Professors Satoyuki Kawano and Kentaro Doi for offering computer facilities for computation. This work is supported by the Grants-in-Aid No. 23360048 and No. 12J02418 from the Japan Society for the Promotion of Science (JSPS).

## APPENDIX: OUTLINE OF NUMERICAL ANALYSIS

In this Appendix, we describe the outline of the numerical analysis based on the semi-Lagrangian method [11]. It utilizes the integrated form (19) for the time increment  $\check{t} - \check{t}_0$  smaller than a certain value, say, the discrete time step. Therefore, it is nothing else than the method of characteristics applied to each time step. Since the upper and lower lines of Eq. (19a) have essentially the same structure, we will explain the method using the upper line.

### 1. Discretized variables

We restrict the space variable  $\check{x}_1$  and molecular velocity  $\check{\zeta}_1$  to finite intervals  $|\check{x}_1| \leq D_{\max}$  and  $|\check{\zeta}_1| \leq Z_{\max}$ , respectively, where  $D_{\max}$  and  $Z_{\max}$  are chosen in such a way that their choice does not affect the final numerical result, and we introduce the discrete time, space, and molecular-velocity variables  $(t^{(n)}, x^{(\pm i)}, \zeta^{(j)})$  for the *transformed* variables  $(\check{t}, \check{x}_1, \check{\zeta}_1)$  [not for the original variables  $(t, x_1, \zeta_1)$ ] as follows:

$$t^{(n)} (n = 0, 1, \dots) \quad \text{with} \quad t^{(0)} = 0, \quad (\text{A1a})$$

$$x^{(\pm i)} (i = 0, 1, \dots, N_x) \quad \text{with} \quad x^{(\pm 0)} = \pm 0, \\ x^{(\pm N_x)} = \pm D_{\max}, \quad (\text{A1b})$$

$$\zeta^{(j)} (j = -N_\zeta, \dots, N_\zeta) \quad \text{with} \quad \zeta^{(0)} = 0, \\ \zeta^{(\pm N_\zeta)} = \pm Z_{\max}. \quad (\text{A1c})$$

Then, we define the discretized velocity distribution functions  $g^{(i,j,n)}$  and  $h^{(i,j,n)}$  and the macroscopic quantities  $\rho^{(i,n)}$ ,  $u_1^{(i,n)}$ ,  $T^{(i,n)}$ ,  $M_0^{(i,n)}$ ,  $M_1^{(i,n)}$ , and  $M_2^{(i,n)}$  by

$$g^{(i,j,n)} = \check{g}(x^{(i)}, \zeta^{(j)}, t^{(n)}), \quad (\text{A2a})$$

$$h^{(i,j,n)} = \check{h}(x^{(i)}, \zeta^{(j)}, t^{(n)}), \quad (\text{A2b})$$

$$U^{(i,n)} = \check{U}(x^{(i)}, t^{(n)}), \quad \text{where} \quad \check{U} = \check{\rho}, \check{u}_1, \check{T}, M_0, M_1, M_2. \quad (\text{A2c})$$

In addition, we denote

$$x_w^{(n)} = x_w(t^{(n)}), \quad v_w^{(n)} = v_w(t^{(n)}), \quad (\text{A3}) \\ G^{(n)} = G(t^{(n)}), \quad \sigma_{w\pm}^{(n)} = \check{\sigma}_{w\pm}(t^{(n)}).$$

### 2. Grid systems

Let us denote by  $\Delta t^{(n-1)}$  the time step between  $t^{(n-1)}$  and  $t^{(n)}$ , i.e.,  $\Delta t^{(n-1)} = t^{(n)} - t^{(n-1)}$ . The  $\Delta t^{(n-1)}$  is not necessarily a constant and can be taken large for large  $n$ , since the time variation of physical quantities such as  $x_w$  and  $\check{g}$  becomes small for large time. In the present paper, we let  $\Delta t^{(n)}$  be 0.01 for the initial stage and increasing gradually until 0.1 as time proceeds.

As for  $x^{(i)}$  and  $\zeta^{(j)}$ , we use nonuniform grid systems that are designed in such a way that the grid size is small when  $|i|$  (or  $|j|$ ) is small and approach a certain value when  $|i|$  (or  $|j|$ ) becomes large. The grid points  $x^{(i)}$  for the space variable are defined by

$$x^{(0)} = 0, \quad x^{(i)} = \frac{i}{|i|} a_x \left( |i| - b_x + \frac{b_x^2}{|i| + b_x} \right) \quad (i \neq 0), \quad (\text{A4})$$

with appropriate positive constants  $a_x$  and  $b_x$ . The grid points  $\zeta^{(j)}$  for the velocity variable are defined by

$$\zeta^{(0)} = 0, \quad \zeta^{(j)} = \begin{cases} \frac{j}{|j|} a_\zeta (|j| - b_\zeta + \frac{b_\zeta^2}{|j| + b_\zeta}) & \text{for even } j, \\ \frac{1}{2} (\zeta^{(j+1)} + \zeta^{(j-1)}) & \text{for odd } j, \end{cases} \quad (\text{A5})$$

with appropriate positive constants  $a_\zeta$  and  $b_\zeta$ . If we do not limit the range of  $i$  (or  $j$ ),  $a_x$  (or  $a_\zeta$ ) is the limiting grid size when  $|i| \rightarrow \infty$  (or  $|j| \rightarrow \infty$ ), and  $b_x$  (or  $b_\zeta$ ) determines the ratio of  $a_x$  (or  $b_x$ ) to the minimum grid size (e.g.,  $x^{(1)} - x^{(0)}$ ). Our reference grid systems are based on the following choices:  $a_x = 1$ ,  $b_x = 9999$ ,  $a_\zeta = 0.2$ , and  $b_\zeta = 1998$ . The numerical results presented in the main text are obtained with this reference grid system unless otherwise stated.

In addition, in the present paper, we let  $N_x = 16\,500$  and  $N_\zeta = 262$ , so that we have  $D_{\max} = 10\,273$  and  $Z_{\max} = 6.074$ . In this case, the smallest grid sizes are  $x^{(1)} - x^{(0)} = 1 \times 10^{-4}$  and  $\zeta^{(1)} - \zeta^{(0)} = 2 \times 10^{-4}$ , and the largest grid sizes are  $x^{(N_x)} - x^{(N_x-1)} = 8.576 \times 10^{-1}$  and  $\zeta^{(N_\zeta)} - \zeta^{(N_\zeta-1)} = 4.354 \times 10^{-2}$ .

### 3. Flow of the numerical analysis

Suppose that everything has been obtained up to time  $t^{(n-1)}$ . We will explain the procedure to obtain the quantities at  $t^{(n)} = t^{(n-1)} + \Delta t^{(n-1)}$ , i.e.,  $x_w^{(n)}$ ,  $v_w^{(n)}$ ,  $\sigma_{w\pm}^{(n)}$ ,  $G^{(n)}$ ,  $g^{(i,j,n)}$ ,  $\rho^{(i,n)}$ ,  $u_1^{(i,n)}$ , and  $T^{(i,n)}$ . Our method is the so-called predictor corrector method. That is, we first compute the predicted quantities by a lower-order method and extrapolation [see Eqs. (A6) and (A8) below] and then compute the corrected values, without extrapolation, by a suitable higher-order method using the predicted values. Predicted quantities are expressed with a  $\hat{\phantom{x}}$  (hat).

(A) Prediction of the trajectory of the plate. Using Eq. (11a), compute  $\hat{x}_w^{(n)}$  and  $\hat{v}_w^{(n)}$  by the Euler forward method:

$$\begin{aligned}\hat{x}_w^{(n)} &= x_w^{(n-1)} + \Delta t^{(n-1)} v_w^{(n-1)}, \\ \hat{v}_w^{(n)} &= v_w^{(n-1)} + \Delta t^{(n-1)} \left[ -x_w^{(n-1)} - \frac{G^{(n-1)}}{\mathcal{M}} \right],\end{aligned}\tag{A6}$$

$$\check{t}_0 = \begin{cases} \tau := \text{largest } s \\ \text{(if } s \in [t^{(n-1)}, t^{(n)}] \text{ such that } W(s; x^{(i)}, \zeta^{(j)}, t^{(n)}) = \pm 0 \text{ exists for } x^{(i)} \geq 0), \\ t^{(n-1)} \text{ (otherwise).} \end{cases}\tag{A9}$$

That is, we let  $\check{t}_0 = \tau$  if the characteristic curve hits the plate during the time interval  $[t^{(n-1)}, t^{(n)}]$  [see Fig. 9(a)] and  $\check{t}_0 = t^{(n-1)}$  otherwise [see Fig. 9(b)]. For  $(i, j)$  for which the boundary condition is applied, we simply put  $\check{t}_0 = t^{(n)}$ . Note that, although  $\check{t}_0$  depends on  $i$ ,  $j$ , and  $n$ , the corresponding superscripts are omitted. The major difference between the semi-Lagrangian method and the method of characteristics [10] lies here: In the latter method, we trace back the characteristic curve until it either hits the plate or reaches the initial time, whereas in the former method we trace back the characteristic curve until  $\check{t} = t^{(n-1)}$  at most. The equation  $W(s; x^{(i)}, \zeta^{(j)}, t^{(n)}) = \pm 0$  in Eq. (A9) becomes a cubic equation if we use the approximation (A7), which can be solved numerically by the Durand-Kerner method [24].

and construct the cubic polynomial  $\hat{\psi}^{(n-1)}(\check{t})$  that interpolates  $x_w(\check{t})$  in  $\check{t} \in [t^{(n-1)}, t^{(n)}]$ :

$$\begin{aligned}\hat{\psi}^{(n-1)}(\check{t}) &= \sum_{l=0}^3 \hat{a}_{n-1,l} (\check{t} - t^{(n-1)})^l, \\ \hat{a}_{n-1,0} &= x_w^{(n-1)}, \quad \hat{a}_{n-1,1} = v_w^{(n-1)}, \\ \hat{a}_{n-1,2} &= \frac{3}{[\Delta t^{(n-1)}]^2} (\hat{x}_w^{(n)} - x_w^{(n-1)}) \\ &\quad - \frac{1}{\Delta t^{(n-1)}} (\hat{v}_w^{(n)} + 2v_w^{(n-1)}), \\ \hat{a}_{n-1,3} &= \frac{2}{[\Delta t^{(n-1)}]^3} (x_w^{(n-1)} - \hat{x}_w^{(n)}) \\ &\quad + \frac{1}{[\Delta t^{(n-1)}]^2} (\hat{v}_w^{(n)} + v_w^{(n-1)}).\end{aligned}\tag{A7}$$

Here, the four coefficients  $\hat{a}_{n-1,0}$ ,  $\hat{a}_{n-1,1}$ ,  $\hat{a}_{n-1,2}$ , and  $\hat{a}_{n-1,3}$  have been determined in such a way that  $\hat{\psi}^{(n-1)}(\check{t})$  and  $d\hat{\psi}^{(n-1)}(\check{t})/d\check{t}$  coincide with  $x_w^{(n-1)}$  and  $v_w^{(n-1)}$  at  $\check{t} = t^{(n-1)}$  and with  $x_w^{(n)}$  and  $v_w^{(n)}$  at  $\check{t} = t^{(n)}$ .

(B) Some other predictions. Approximate the values on the boundary  $\hat{\sigma}_{w\pm}^{(n)}$ ,  $\hat{\rho}^{(\pm 0, n)}$ , and  $\hat{T}^{(\pm 0, n)}$  as

$$\begin{aligned}\hat{\sigma}_{w\pm}^{(n)} &= \check{\sigma}_{\text{eq}\pm}(\hat{v}_w^{(n)}) - \check{\sigma}_{\text{eq}\pm}(v_w^{(n-1)}) + \sigma_{w\pm}^{(n-1)}, \\ \hat{\rho}^{(\pm 0, n)} &= \rho^{(\pm 0, n-1)}, \quad \hat{T}^{(\pm 0, n)} = T^{(\pm 0, n-1)}.\end{aligned}\tag{A8}$$

(C) Prediction of the velocity distribution function. In this step, we compute the prediction of the velocity distribution function  $\hat{g}^{(i,j,n)}$  (and  $\hat{h}^{(i,j,n)}$ ) by the use of Eq. (19a) and the macroscopic quantities  $\rho^{(i,n)}$ ,  $u_1^{(i,n)}$ , and  $T^{(i,n)}$ .

First we describe the procedure to obtain the value at the ‘‘foot’’ of characteristic curve, i.e.,  $\check{g}(W(\check{t}_0; \check{x}_1, \check{\zeta}_1, \check{t}), Z(\check{t}_0; \check{x}_1, \check{\zeta}_1, \check{t}), \check{t}_0)$ . For all  $i = \pm 0, \dots, \pm N_x$  and  $j = 0, \dots, \pm N_\zeta$  except for  $(i, j)$  such that  $x^{(i)} = \pm 0$  and  $\zeta^{(j)} \geq 0$  [that is,  $(i, j)$  for which the boundary condition is applied], trace back the corresponding characteristic curve [Eq. (19b)] to the past and define  $\check{t}_0$  as follows:

This method is more stable than the Newton method. Then, from (19b) and (19c), we have the position  $x_{\#}^{(j)}$  of the foot of the characteristic curve and the corresponding molecular velocity  $\zeta_{\#}^{(j)}$ , i.e.,

$$\begin{aligned}x_{\#}^{(j)} &= W(\check{t}_0; x^{(i)}, \zeta^{(j)}, t^{(n)}) \quad \text{and} \\ \zeta_{\#}^{(j)} &= Z(\check{t}_0; x^{(i)}, \zeta^{(j)}, t^{(n)}).\end{aligned}\tag{A10}$$

Note that, although  $x_{\#}^{(j)}$  and  $\zeta_{\#}^{(j)}$  depend also on  $i$  and  $n$ , the corresponding superscripts are omitted. We now let

$$\begin{aligned}U_{\#}^{(j)} &= \check{U}(x_{\#}^{(j)}, \check{t}_0), \quad g_{\#}^{(j)} = \check{g}(x_{\#}^{(j)}, \zeta_{\#}^{(j)}, \check{t}_0), \\ h_{\#}^{(j)} &= \check{h}(x_{\#}^{(j)}, \zeta_{\#}^{(j)}, \check{t}_0),\end{aligned}\tag{A11}$$

and compute  $U_{\#}^{(j)}$ ,  $g_{\#}^{(j)}$ , and  $h_{\#}^{(j)}$  by the following procedure.

case a. If  $|\zeta_{\#}^{(j)}| > Z_{\max}$  or  $|x_{\#}^{(j)}| > D_{\max}$ , that is, if  $x_{\#}^{(j)}$  and  $\zeta_{\#}^{(j)}$  are outside the respective computational domains, use the values at the reference state for  $\rho_{\#}^{(j)}$ ,  $u_{1\#}^{(j)}$ ,  $T_{\#}^{(j)}$ , and  $g_{\#}^{(j)}$ :

$$\rho_{\#}^{(j)} = 1, \quad u_{1\#}^{(j)} = -v_w(\check{t}_0), \quad T_{\#}^{(j)} = 1, \quad g_{\#}^{(j)} = h_{\#}^{(j)} = 0. \quad (\text{A12})$$

case b. If  $|\zeta_{\#}^{(j)}| \leq Z_{\max}$  and  $|x_{\#}^{(j)}| \leq D_{\max}$ , and if  $x_{\#}^{(j)} = \pm 0$  (or equivalently  $\check{t}_0 = \tau$ ), that is, if the foot of the characteristic curve is on the plate [see Fig. 9(a)], we use the following linear interpolation to obtain the macroscopic quantities  $\rho_{\#}^{(j)}$ ,  $u_{1\#}^{(j)}$ , and  $T_{\#}^{(j)}$ :

$$\mathcal{H}_{\#}^{(j)} = \hat{\mathcal{H}}^{(\pm 0, n)} \frac{\tau - t^{(n-1)}}{\Delta t^{(n-1)}} - \mathcal{H}^{(\pm 0, n-1)} \frac{\tau - t^{(n)}}{\Delta t^{(n-1)}} \quad (\mathcal{H} = \rho, T),$$

$$u_{1\#}^{(j)} = 0. \quad (\text{A13})$$

[Note that Eq. (A13), which is prepared for process (F) below, becomes trivial in the present process of prediction because of Eq. (A8).] As for the velocity distribution function  $g_{\#}^{(j)}$ , we use boundary condition (17) with the following linear interpolation [see Eq. (17)]:

$$g_{\#}^{(j)} = h_{\#}^{(j)} = \sigma_{w_{\#}^{\pm}}^* E(\zeta_{\#}^{(j)}) - E(\zeta_{\#}^{(j)} + v_w(\tau)), \quad (\text{A14a})$$

$$\sigma_{w_{\#}^{\pm}}^* = \hat{\sigma}_{w_{\pm}}^{(n)} \frac{\tau - t^{(n-1)}}{\Delta t^{(n-1)}} - \sigma_{w_{\pm}}^{(n-1)} \frac{\tau - t^{(n)}}{\Delta t^{(n-1)}}. \quad (\text{A14b})$$

case c. If otherwise, that is, if  $x_{\#}^{(j)}$  and  $\zeta_{\#}^{(j)}$  are in the respective computational domains [see Fig. 9(b)], we can obtain the following values at the foot of the characteristic curve:

$$\rho_{\#}^{(j)} = \check{\rho}(x_{\#}^{(j)}, t^{(n-1)}), \quad u_{1\#}^{(j)} = \check{u}_1(x_{\#}^{(j)}, t^{(n-1)}),$$

$$T_{\#}^{(j)} = \check{T}(x_{\#}^{(j)}, t^{(n-1)}), \quad (\text{A15a})$$

$$g_{\#}^{(j)} = \check{g}(x_{\#}^{(j)}, \zeta_{\#}^{(j)}, t^{(n-1)}), \quad h_{\#}^{(j)} = \check{h}(x_{\#}^{(j)}, \zeta_{\#}^{(j)}, t^{(n-1)}), \quad (\text{A15b})$$

by interpolation using the known quantities in the previous step  $t = t^{(n-1)}$ :

$$\rho^{(i, n-1)}, \quad u_1^{(i, n-1)}, \quad T^{(i, n-1)}, \quad g^{(i, j, n-1)}, \quad h^{(i, j, n-1)},$$

for  $i = \pm 0, \dots, \pm N_x$ ,  $j = 0, \dots, \pm N_z$ . (A16)

Here, the third-order ENO interpolation [25] is employed.

$$\hat{g}^{(i, j, n)} = g_{\#}^{(j)} + \gamma [Q_g(x_{\#}^{(j)}, \zeta_{\#}^{(j)}, \check{t}_0) + Q_g(x^{(i)}, \zeta^{(j)}, t^{(n)})] = g_{\#}^{(j)} + \gamma \{ \rho_{\#}^{(j)} [M_{\#}^{(j)} - E(\zeta_{\#}^{(j)}) - g_{\#}^{(j)}] + \rho^{(i, n)} [M^{(i, j, n)} - E(\zeta^{(j)}) - \hat{g}^{(i, j, n)}] \}, \quad (\text{A19a})$$

$$\gamma = \frac{1}{\mathbf{K}} \frac{t^{(n)} - \check{t}_0}{2}, \quad \tilde{\zeta}_{\#}^{(j)} = \zeta_{\#}^{(j)} + v_w(\check{t}_0), \quad \tilde{\zeta}^{(j)} = \zeta^{(j)} + \hat{v}_w^{(n)}, \quad (\text{A19b})$$

$$M_{\#}^{(j)} = \check{M}(x_{\#}^{(j)}, \zeta_{\#}^{(j)}, \check{t}_0), \quad M^{(i, j, n)} = \check{M}(x^{(i)}, \zeta^{(j)}, t^{(n)}), \quad (\text{A19c})$$

to obtain the predicted value  $\hat{g}^{(i, j, n)}$  as

$$\hat{g}^{(i, j, n)} = \frac{(1 - \rho_{\#}^{(j)}) \gamma g_{\#}^{(j)} + \gamma \{ \rho_{\#}^{(j)} [M_{\#}^{(j)} - E(\zeta_{\#}^{(j)})] + \rho^{(i, n)} [M^{(i, j, n)} - E(\zeta^{(j)})] \}}{1 + \rho^{(i, n)} \gamma}. \quad (\text{A20})$$

The predicted value  $\hat{h}^{(i, j, n)}$  is obtained similarly.

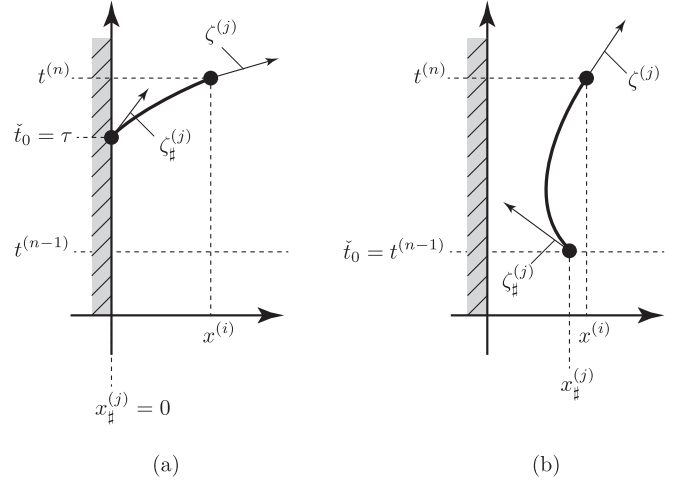


FIG. 9. Schematic figure for the definition of  $\check{t}_0$ . (a) The case where the characteristic curve hits the plate during the time interval  $[t^{(n-1)}, t^{(n)}]$ ; (b) the case other than (a).

Before working on Eq. (19a), we compute the macroscopic quantities at  $\check{t} = t^{(n)}$  using the conservation laws (20), which can be written in the following discretized form:

$$\mathbf{M}_0^{(i, n)} = \sum_{j=-N_z}^{N_z} g_{\#}^{(j)} w^{(j)}, \quad \mathbf{M}_1^{(i, n)} = \sum_{j=-N_z}^{N_z} \zeta_{\#}^{(j)} g_{\#}^{(j)} w^{(j)}, \quad (\text{A17})$$

$$\mathbf{M}_2^{(i, n)} = \sum_{j=-N_z}^{N_z} [\zeta_{\#}^{(j)}]^2 g_{\#}^{(j)} w^{(j)} + \sum_{j=-N_z}^{N_z} h_{\#}^{(j)} w^{(j)},$$

where  $w^{(j)}$  is the weight determined by the quadrature (Simpson's rule is used for the actual computation). Then, Eq. (21) gives

$$\rho^{(i, n)} = 1 + \mathbf{M}_0^{(i, n)}, \quad u_1^{(i, n)} = \frac{1}{\rho^{(i, n)}} (\mathbf{M}_1^{(i, n)} - \hat{v}_w^{(n)}),$$

$$T^{(i, n)} = \frac{2}{3\rho^{(i, n)}} \left( \mathbf{M}_2^{(i, n)} + \frac{3}{2} + [\hat{v}_w^{(n)}]^2 - \rho^{(i, n)} [u_1^{(i, n)}]^2 \right). \quad (\text{A18})$$

In this way, we can obtain the macroscopic quantities at  $\check{t} = t^{(n)}$  before computing the velocity distribution functions  $\check{g}$  and  $\check{h}$  at  $\check{t} = t^{(n)}$  [11, 26, 27].

Then, we discretize (19a) using the trapezoidal rule (second order in time):

(D) Prediction of the boundary condition and the drag force. We compute the prediction  $\hat{\sigma}_{w\pm}^{(n)}$  of  $\check{\sigma}_{w\pm}$  in the boundary condition and the prediction  $\hat{G}^{(n)}$  of the drag force using the discretized versions of Eqs. (17b) and (18):

$$\begin{aligned}\hat{\sigma}_{w\pm}^{(n)} &= \check{\sigma}_{\text{eq}\pm}(\hat{v}_w^{(n)}) \mp 2\sqrt{\pi}A_{1\pm}, \\ \hat{G}^{(n)} &= A_{2+} + A_{3+} - A_{2-} - A_{3-},\end{aligned}\quad (\text{A21})$$

where

$$\begin{aligned}A_{1\pm} &= \sum_{j=0, \mp 1, \dots, \mp N_c} \zeta^{(j)} \hat{g}^{(\pm 0, j, n)} w_{\pm}^{(j)} \\ &\left( \simeq \int_{\check{\zeta}_1 \leq 0} \check{\zeta}_1 \check{g}(\pm 0, \check{\zeta}_1, \check{t}) d\check{\zeta}_1 \right),\end{aligned}\quad (\text{A22a})$$

$$\begin{aligned}A_{2\pm} &= \sum_{j=0, \mp 1, \dots, \mp N_c} [\zeta^{(j)}]^2 \hat{g}^{(\pm 0, j, n)} w_{\pm}^{(j)} \\ &\left( \simeq \int_{\check{\zeta}_1 \leq 0} \check{\zeta}_1^2 \check{g}(\pm 0, \check{\zeta}_1, \check{t}) d\check{\zeta}_1 \right),\end{aligned}\quad (\text{A22b})$$

$$\begin{aligned}A_{3\pm} &= \frac{1}{4} [\hat{\sigma}_{w\pm}^{(n)} - 1 \pm \text{erf}(\hat{v}_w^{(n)})] \pm \frac{\hat{v}_w^{(n)}}{2\sqrt{\pi}} \exp(-[\hat{v}_w^{(n)}]^2) \\ &- \frac{[\hat{v}_w^{(n)}]^2}{2} \text{erfc}(\pm \hat{v}_w^{(n)}) \left( \simeq \int_{\check{\zeta}_1 \geq 0} \check{\zeta}_1^2 \check{g}(\pm 0, \check{\zeta}_1, \check{t}) d\check{\zeta}_1 \right) \\ &= \int_{\check{\zeta}_1 \geq 0} \check{\zeta}_1^2 [\check{\sigma}_{w\pm}(\check{t}) E(\check{\zeta}_1) - E(\check{\zeta}_1 + v_w(\check{t}))] d\check{\zeta}_1,\end{aligned}\quad (\text{A22c})$$

where  $w_{\pm}^{(j)}$  is the weight determined by the quadrature (Simpson's rule is used for the actual computation). In the parentheses in Eq. (A22c), use is made of Eq. (17). Note that  $\hat{\sigma}_w^{(n)}$  is updated by the first equation in Eq. (A21).

(E) Correction of the trajectory of the plate. Once  $\hat{G}^{(n)}$  is obtained, we can compute the corrected values of  $x_w^{(n)}$  and  $v_w^{(n)}$  by using the trapezoidal rule in Eq. (11a):

$$x_w^{(n)} = x_w^{(n-1)} + \Delta t^{(n-1)} \frac{\hat{v}_w^{(n)} + v_w^{(n-1)}}{2}, \quad (\text{A23a})$$

$$v_w^{(n)} = v_w^{(n-1)} + \Delta t^{(n-1)} \frac{1}{2} \left[ -\hat{x}_w^{(n)} - \frac{\hat{G}^{(n)}}{\mathcal{M}} - x_w^{(n-1)} - \frac{G^{(n-1)}}{\mathcal{M}} \right]. \quad (\text{A23b})$$

Then, we construct the cubic polynomial  $\psi^{(n-1)}$  (for corrected values) that interpolates  $x_w(\check{t})$  for  $\check{t} \in [t^{(n-1)}, t^{(n)}]$  as in process (A).

(F) Correction of the velocity distribution function. Repeat process (C) with suitable changes from the predicted values to the corrected ones. To be more specific, the cubic polynomial  $\psi^{(n-1)}$  constructed in process (E) is used in place of  $\hat{\psi}^{(n-1)}$  in solving  $W(s; x^{(i)}, \zeta^{(j)}, t^{(n)}) = \pm 0$  (this change affects all the quantities with  $\sharp$  [e.g., Eq. (A10)] and quantities computed from them [e.g., Eq. (A17)]);  $\hat{\sigma}_{w\pm}^{(n)}$  updated in Eq. (A21) is used in Eq. (A14b);  $\hat{\mathcal{H}}^{(\pm 0, n)}$  is replaced with  $\mathcal{H}^{(\pm 0, n)}$  in Eq. (A13);  $g^{(i, j, n)}$ , the corrected value to be obtained, replaces  $\hat{g}^{(i, j, n)}$  in Eqs. (A19a) and (A20), and  $v_w^{(n)}$  replaces  $\hat{v}_w^{(n)}$  in Eq. (A19b).

(G) Correction of the boundary condition and the drag force. Repeat process (D) with suitable changes from the predicted values to the corrected ones as in process (F) to obtain the corrected values  $\sigma_{w\pm}^{(n)}$  and  $G^{(n)}$ .

- 
- [1] S. Caprino, G. Cavallaro, and C. Marchioro, *Math. Models Methods Appl. Sci.* **17**, 1369 (2007).
- [2] T. Tsuji and K. Aoki, in *27th International Symposium on Rarefied Gas Dynamics, 2010*, AIP Conf. Proc. No. 1333, edited by D. A. Levin, I. J. Wysong, and A. L. Garcia (AIP, Melville, 2011), p. 140.
- [3] T. Tsuji and K. Aoki, *J. Stat. Phys.* **146**, 620 (2012).
- [4] S. Caprino, C. Marchioro, and M. Pulvirenti, *Commun. Math. Phys.* **264**, 167 (2006).
- [5] G. Cavallaro, *Rend. Mat. Appl.* **27**, 123 (2007).
- [6] K. Aoki, G. Cavallaro, C. Marchioro, and M. Pulvirenti, *Math. Modell. Numer. Anal.* **42**, 263 (2008).
- [7] K. Aoki, T. Tsuji, and G. Cavallaro, *Phys. Rev. E* **80**, 016309 (2009).
- [8] P. L. Bhatnagar, E. P. Gross, and M. Krook, *Phys. Rev.* **94**, 511 (1954).
- [9] P. Welander, *Arkiv Fysik* **7**, 507 (1954).
- [10] T. Tsuji and K. Aoki, *J. Comput. Phys.* **250**, 574 (2013).
- [11] G. Russo and F. Filbet, *Kinet. Relat. Models* **2**, 231 (2009).
- [12] M. N. Kogan, *Rarefied Gas Dynamics* (Plenum, New York, 1969).
- [13] C. Cercignani, *The Boltzmann Equation and Its Applications* (Springer, New York, 1988).
- [14] Y. Sone, *Molecular Gas Dynamics: Theory, Techniques, and Applications* (Birkhäuser, Boston, 2007).
- [15] G. Dechristé and L. Mieussens, in *28th International Symposium on Rarefied Gas Dynamics, 2012*, AIP Conf. Proc. No. 1501, edited by M. Mareschal and A. Santos (AIP, Melville, 2012), p. 366.
- [16] G. Dechristé and L. Mieussens, *J. Phys. Conf. Ser.* **362**, 012030 (2012).
- [17] S. Chen, K. Xu, C. Lee, and Q. Cai, *J. Comput. Phys.* **231**, 6643 (2012).
- [18] C. K. Chu, *Phys. Fluids* **8**, 12 (1965).
- [19] T. Tsuji and K. Aoki, in *28th International Symposium on Rarefied Gas Dynamics, 2012*: AIP Conf. Proc. 1501, edited by M. Mareschal and A. Santos (AIP, Melville, 2012), p. 115.
- [20] G. Cavallaro and C. Marchioro, *Math. Models Methods Appl. Sci.* **20**, 1999 (2010).
- [21] E. Kestemont, C. Van den Broeck, and M. M. Mansour, *Europhys. Lett.* **49**, 143 (2000).
- [22] N. Chernov and J. L. Lebowitz, *J. Stat. Phys.* **109**, 507 (2002).
- [23] E. Caglioti, N. Chernov, and J. L. Lebowitz, *Nonlinearity* **17**, 897 (2004).
- [24] O. Aberth, *Math. Comput.* **27**, 339 (1973).

- [25] C.-W. Shu, in *Advanced Numerical Approximation of Nonlinear Hyperbolic Equations*, edited by B. Cockburn, C. Johnson, C.-W. Shu, and E. Tadmor, Lecture Notes in Mathematics Vol. 1697 (Springer, Berlin, 1998), p. 325.
- [26] F. Coron and B. Perthame, *SIAM J. Numer. Anal.* **28**, 26 (1991).
- [27] S. Pieraccini and G. Puppo, *J. Sci. Comput.* **32**, 1 (2007).